Miniaturization Design for SRM Satisfying the Requirements of N-T characteristic Focusing Magnetic Saturation

Takahiro Kumagai [1*], Jun-ichi Itoh [1], Keisuke Kusaka [1], and Daisuke Sato [2]
[1] Department of Electrical, Electronics and Information Engineering, Nagaoka University of Technology, Japan
[2] Nagaoka Motor Development Co., Ltd., Japan

***Abstract*—This paper proposes a miniaturization design method for a switched reluctance motor from the requirement of N-T characteristic. In particular, a specific parameter related to magnetic saturation is defined in order to arbitrarily determine how much to use the magnetic properties of the iron core material. Typical motor dimensions are obtained by setting the parameter related to magnetic saturation, maximum electrical frequency, maximum current density, maximum copper loss, conductor slot fill factor, magnetic properties of material, and input voltage. The designed motor is analyzed by a Finite Element Method in order to validate the proposed method.**

***Index Terms*—Switched reluctance motor (SRM), motor design, N-T characteristic, magnetic saturation**

I. INTRODUCTION

High-efficiency and high-power density motor have been studied actively [1-2]. With the improvement of motor design and magnetic material, high power density and efficiency of switched reluctance motor (SRM) are reported to be competitive to those of magnet motor [3].

In order to determine the typical motor diameters such as stack thickness, stator outer diameter, and rotor outer diameter, a traditional design method based on output equation of output density and output coefficient is widely used [4]. In this method, first, the output density and the output coefficient are determined, next, the typical motor diameters are back-calculated from the required torque and output. The determination of these coefficients relies on designer's experience or past design example due to its dependencies on many factors such as the type and structure of the motor, the kind of the iron core material, and winding current. However, it is difficult for SRM's design to rely on the designer's experience and the past design example because (i) magnetic saturation is used actively unlike typical motor and (ii) new magnetic material is being developed. Inappropriate determination of these coefficients leads to not only low efficiency and low power density but also design rework due to the dissatisfaction of the required N-T characteristics.

This paper proposes the design method to satisfy the required N-T characteristic and to realize the miniaturized motor volume considering the magnetic properties. In particular, the specific parameter related to the magnetic saturation is defined in order to arbitrarily determine how much to use the magnetic properties of the iron material.

II. PROSED DESIGN METHOD

Fig. 1 shows a N-T characteristic. The N-T characteristic is determined by the rated output P_{out}, maximum rotation speed ω_{max}, and base speed ω_{base}. The maximum torque $T_{max}(=P_{out}/\omega_{base})$ and the torque at maximum speed $T_{\omega max}(=P_{out}/\omega_{max})$ are uniquely determined from P_{out}, ω_{base}, ω_{max}. Generally, a rectangular current waveform drive is employed at lower ω_{base}, whereas a single pulse drive is employed at higher ω_{base}.

Fig.2 shows the SRM shape. In this paper, number of phases m, number of stator poles N_r and rotor poles N_s, stack thickness L_h, stator outer diameter D_s, rotor outer diameter D_r, and number of turns N are designed to satisfy the required N-T characteristic and to realize the miniaturized motor volume. The airgap length l_g is determined by structural restrictions. In addition, the stator's and rotor's pole width t_s, t_r are calculated by these pole arc angle β_s, β_r determined by the Corda triangle [4], whereas stator yoke thickness y_s, rotor slot depth d_r, and shaft diameter r_{sh} are determined in order to avoid extreme magnetic saturation [4]. Note that the magnetic flux flowing on the teeth's side is ignored for simplification.

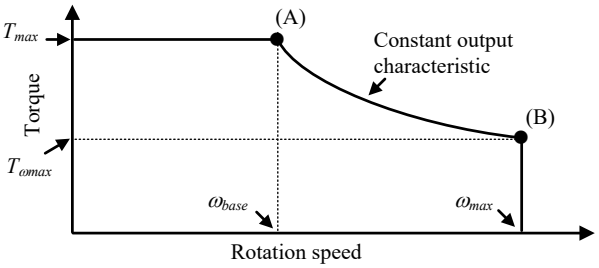

Fig. 1 Output N-T characteristics

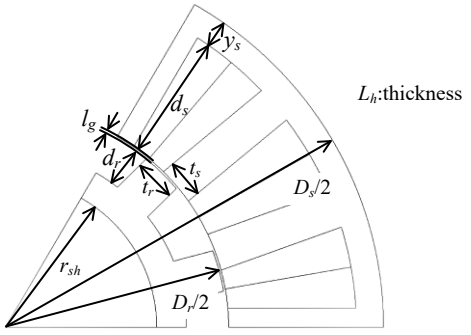

Fig. 2 Dimensions of SRM

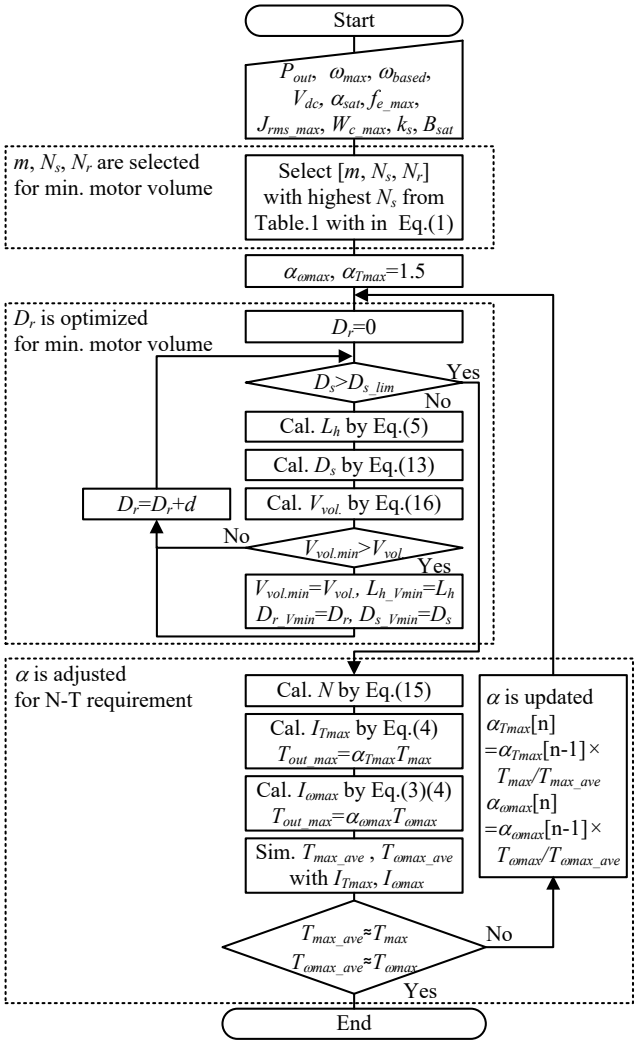

Fig. 3 Proposed design flow of SRM

Fig.3 shows the miniaturization design algorithm satisfying the required N-T characteristic. As a input constants, there are eight variables; desired N-T characteristic (operating point (A) and (B) in Fig.1), input voltage V_{dc}, saturation level α_{sat}, maximum electrical frequency f_{e_max}, maximum current density J_{rms_max}, maximum copper loss W_{c_max}, conductor slot fill factor k_s, and saturation magnetic density B_{sat}. The motor diameters are derived from the following the input constants or the optimization condition in each section.

Section A m, N_s, N_r: operating point (B) and f_{e_max}
Section B L_h: operating point (A) and α_{sat}
Section C D_s: operating point (A), J_{rms_max}, W_{c_max}, k_s
Section D N: operating point (A) or (B), V_{dc}
Section E D_r: minimization of motor volume

In addition, α_{Tmax}, $\alpha_{\omega max}$ are the adjustment parameters for satisfaction of the required N-T characteristic, and these adjustment method are explained in section F.

A. Number of Phases and Poles m, N_s, N_r

Table 1 shows the typical combinations of the phase-numbers and the pole-numbers and the examples of these applications. Selection of higher N_s leads to miniaturization of motor volume thanks to reduction of the stator yoke thickness and the coil-end length. Therefore, the combination with highest N_s is selected within the range where electrical frequency at ω_{max} does not exceed f_{e_max}; the range is expressed by (1).

TABLE I
COMBINATIONS OF PHASE-NUMBERS AND POLE-NUMBERS

	m	N_s	N_r	λ [4]	Example of application [5]
Selection of highest N_s within eq.(1)	3	6	4	High	supercharger, micro-machine
	4	8	6	High	servo
	3	12	8	High	pump, off-road vehicle
	4	16	12	Low	traction, UAV
	3	18	12	Low	electric vehicle
Not covered	Higher			Lower	electric vehicle

λ: inductance ratio = unsaturated aligned inductance / unaligned inductance, UAV: unmanned aerial vehicle

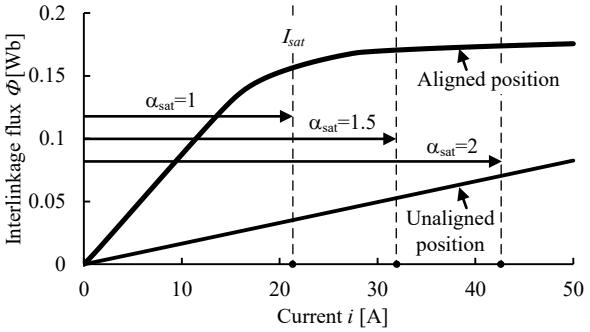

Fig.4 Relationship between current amplitude and magnetization characteristic

$$N_r \le \frac{2\pi f_{e\_\max}}{\omega_{\max}} \quad \text{.....(1)}$$

Note that the selection of higher N_s also leads to increase of the magnetic flux flowing on the side of the teeth. This results in high unaligned inductance, i.e. low inductance ratio λ. In the proposed method, optimum design considering its magnetic flux cannot be conducted because it is ignored for simplification. According to Ref.[4], the λ is decreased from four-phase 16-12 type and three-phase 18-12 type. Therefore, the three-phase 18-12 type is the limit for the proposed design method ignoring the magnetic flux flowing on the side of the teeth. Since the SRM with relatively low N_s is used for low and medium power application as shown in Table 1, the proposed design's target will be low and medium power application.

B. Stack Thickness L_h

Fig.4 shows the relationship between the current amplitude and the magnetization characteristic. The proposed method firstly defines the parameter α_{sat} as (2).

$$\alpha_{sat} = \frac{I_{T\max}}{I_{sat}} \qquad where \;\; I_{sat} = \frac{B_{sat} l_g}{N\mu_0} \quad \text{.....(2)}$$

where I_{Tmax} is the amplitude of the current reference at the maximum torque and μ_0 is space permeability. The magnetic flux density in the airgap reaches B_{sat} at the current of I_{sat}, i.e. I_{sat} is saturation start point. Therefore, α_{sat} is the parameter to determine how much to use the magnetic properties from the saturation start point.

The instantaneous maximum torque under magnetic linear region, i.e. $i \le I_{sat}$, is expressed as (3).

$$T_{out\_\max} = \frac{N_s}{m}\frac{1}{2}\frac{N^2\mu_0 L_h\left(\frac{D_r}{2}\right)}{l_g} i^2 \quad \text{.....(3)}$$

On the other hand, the instantaneous maximum torque under magnetic saturation region, i.e. $i \geq I_{sat}$, is expressed as (4).

$$T_{out\_\max} = \frac{N_s}{m} N B_{sat} L_h \left(\frac{D_r}{2}\right)(i - \frac{1}{2} I_{sat}) \quad \text{.....(4)}$$

Fig.5 shows the comparison of the instantaneous maximum torque between the theoretical value calculated by (3) and (4) and the FEM results. As shown in Fig.5, the theoretical value is the almost same as the FEM results. The average torque is smaller than the instantaneous maximum torque due to the torque ripple. In this paper, the ratio of the instantaneous maximum torque to the average torque is defined as $\alpha_{Tmax}=T_{max\_max}/T_{max}$ at operating point (a). Assuming with $I_{Tmax} \geq I_{sat}$, the stack thickness L_h is expressed as (5) from (2) and (4).

$$L_h = \frac{2m\mu_0\alpha_{T\max}T_{\max}}{N_s D_r B_{sat}{}^2 l_g(\alpha_{sat} - \frac{1}{2})} \quad \text{.....(5)}$$

Selection of higher α_{sat} leads to the reduction of the stack thickness; therefore, the motor volume is reduced by active use of the magnetic properties of the iron material.

C. Stator Outer Diameter D_s

Fig.6 shows the relationship between the speed and the current RMS value. Assuming that the current waveform is the pulsed current with the current amplitude I_{Tmax}, the current RMS value is expressed as (6).

$$I_{RMS} = \sqrt{\frac{1}{T}\int_0^{Td_{T\max}} I_{T\max}{}^2 dt} = I_{T\max}\sqrt{d_{T\max}} \quad \text{.....(6)}$$

where d_{Tmax} is the ratio of the electrical period to the pulse width. As shown in Fig.6, the theoretical value is the almost same as the FEM results.

Fig.7 shows the diagrams of the stator slot. Fig.7 (a) is the stator slot, whereas Fig.7 (b) is a cross section of the stator tooth and winding.

First, the determination method satisfy the maximum current density J_{rms_max} is explained. The slot area per coil (the shaded area in Fig.7(a)) is expressed as (7).

$$S_{slot} = \frac{\pi}{2N_s} d_s^2 + (\frac{\pi}{N_s} - \sin\left(\frac{\beta_s}{2}\right))(\frac{D_r}{2} + l_g) d_s \quad \text{.....(7)}$$

On the other hand, the required slot area per coil S_{slot_J} is expressed as (8) from (2) and (6).

$$S_{slot\_J} = \frac{S_{coil}}{k_s} = \frac{NI_{T\max}\sqrt{d_{T\max}}}{k_s J_{rms\_\max}} = \frac{\sqrt{d_{T\max}}}{k_s J_{rms\_\max}} \frac{\alpha_{sat} B_{sat} l_g}{\mu_0} \quad \text{.....(8)}$$

where S_{coil} is the conductor area (copper core wire area) in the slot. By solving $S_{slot} \geq S_{slot\_J}$ with (7) and (8), the required slot depth d_s can be derived (Omitted due to the page limitation). Note that the minimum slot depth d_s which satisfies $S_{slot} \geq S_{slot\_J}$ is defined as d_{s_J}.

Next, the determination method to satisfy the maximum copper loss W_{c_max} is explained. The copper loss is expressed as (9) from (2) and (6).

$$W_c = N_s \frac{\rho_R L_{coil} N}{k_s S_{coil}/N} I_{RMS}{}^2 = N_s \frac{\rho_R L_{coil}}{k_s S_{coil}} (\alpha_{sat} \frac{B_{sat} l_g}{\mu_0} \sqrt{d_{T\max}})^2 \quad \text{.....(9)}$$

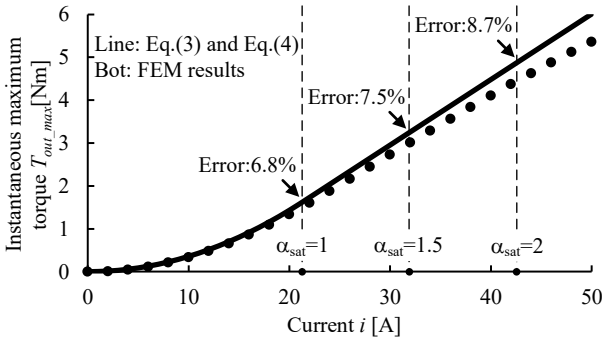

Fig.5 Instantaneous maximum torque

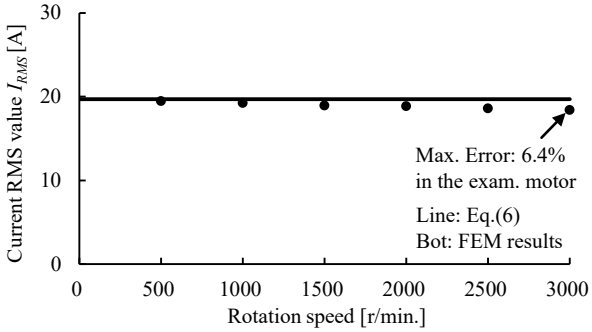

Fig. 6 Relationship between speed and current RMS value (d_{Tmax}=1/3)

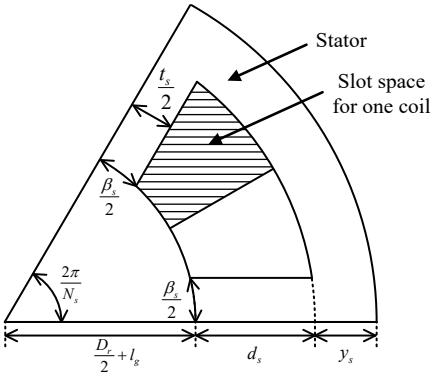

(a) Stator slot of SRM

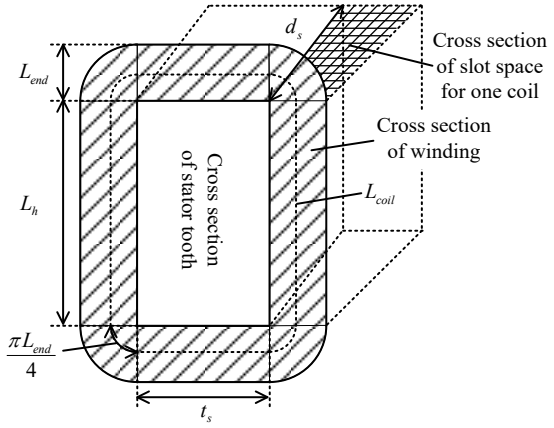

(b) Cross section of stator tooth and winding of SRM

Fig.7 Diagrams of stator slot

where L_{coil} is the average coil length per turn as shown in Fig.7(b), is expressed as (10).

$$L_{coil} = 2L_h + 2t_s + \pi L_{end} \quad \text{.....(10)}$$

$$L_{end} = \frac{S_{slot}}{d_s} = \frac{\pi}{2N_s} d_s + (\frac{\pi}{N_s} - \sin\left(\frac{\beta_s}{2}\right))(\frac{D_r}{2} + l_g) \quad \text{.....(11)}$$

By solving $W_c \le W_{c\_max}$ from (9) to (11), the required slot depth d_s can be derived (Omitted due to the page limitation). Note that the minimum slot depth d_s which satisfies $W_c \le W_{c\_max}$ is defined as d_{s_C}.

In order to reduce the motor volume, the minimum slot depth d_s which satisfies both $S_{slot} \ge S_{slot\_J}$ and $W_c \le W_{c\_max}$ is selected; therefore the slot depth d_s is expressed as (12).

$$d_s = \max(d_{s\_J}, d_{s\_C}) \quad \text{.....(12)}$$

On the other hand, the stator outer diameter D_s is the sum of the rotor outer diameter, the air gap length, the slot depth, and the stator yoke thickness, is expressed as (13)

$$D_s = 2\left\{\frac{D_r}{2} + l_g + m_s\left(\frac{D_r}{2} + l_g\right)\sin\left(\frac{\beta_s}{2}\right) + d_s\right\} \quad \text{.....(13)}$$

D. Number of Turns N

The determination method to avoid higher the back electromotive force (EMF) V_{emf} at base speed than the input voltage V_{dc} is explained. The method of determining from the maximum speed is omitted due to the page limitation. The back EMF V_{emf} at ω_{base} is expressed as (14).

$$V_{emf} = \frac{\partial \Phi_{sat}}{\partial \theta_m}\omega_{base} = \frac{N_s}{m} N B_{sat} L_h \left(\frac{D_r}{2}\right)\omega_{base} \quad \text{.....(14)}$$

By solving $V_{emf} \le V_{dc}$ with (14), the number of turns N is expressed as (15).

$$N \le \frac{m V_{dc}}{N_s B_{sat} L_h \left(\frac{D_r}{2}\right)\omega_{base}} \equiv N_{(A)} \quad \text{.....(15)}$$

Note that the maximum number of turns N which satisfies $V_{emf} \le V_{dc}$ is defined as $N_{(A)}$. In order to reduce the maximum current amplitude for inverter, the maximum number of turns $N_{(A)}$ which satisfies $V_{emf} \le V_{dc}$ is selected.

E. Rotor Outer Diameter D_r

By regarding the motor volume $V_{vol.}$ as the cylinder's volume with the stator diameter and the motor's axial length, the motor volume $V_{vol.}$ is expressed as (16).

$$V_{vol.}(\alpha_{T\max}, D_r) = \frac{\pi}{4} D_s^2 L_{all} = \frac{\pi}{4} D_s^2 (L_h + 2L_{end}) \quad \text{.....(16)}$$

Where L_{all} is the axial length of the motor including the coil-end length. The parameters D_s, L_h, L_{end} in (16) are the function of D_r as explained in the previous sections; however, they are also the function of α_{Tmax} which is the adjustment parameter. Therefore, first, the motor dimensions with initial value of α_{Tmax} are determined by searching for D_r in order to minimize (16), next, the α_{Tmax} is adjusted by FEM. These processes are repeated until achievement of the desired torque.

F. Parameter Adjustment with Simulation

As shown in Fig.3, α_{Tmax} and $\alpha_{\omega max}$ are adjusted by multiplying the previous value of α_{Tamx} and $\alpha_{\omega max}$ by the ratio of the desired torque to the average torque in the simulation. This flow is repeated until the simulated average torque is the almost same as the desired torque. This process is achieved with only few repeats because α_{Tmax} and $\alpha_{\omega max}$ can be accurately adjusted with the use of previously adjusted α_{Tmax} and $\alpha_{\omega max}$. Note that the current reference is back-calculated from (2) or (3), whereas the control parameters of on-angle and off-angle are decided according to Ref.[4].

TABLE II
DESIGN REQUIREMENTS AND CONSTRAINTS.

Design requirements		
Output power	P_{out}	0.75kW
Maximum speed	ω_{max}	5000r/min ($T_{\omega max}$=1.43Nm)
Base speed	ω_{base}	3000r/min (T_{max}=2.39Nm)
Input voltage	V_{dc}	48V
Saturation level	α_{sat}	1.6
Max. electrical frequency	f_{e_max}	2kHz
Max. current density	J_{rms_max}	10A/mm^2
Max. copper loss	W_{c_max}	75W (W_{c_max}/P_{out}=0.1)
Space factor	k_s	50%
Sat. magnetic flux density	B_{sat}	1.64T (35H300)
Design constraints		
Airgap	l_g	0.25mm
Stator pole arc	β_s	10deg.
Rotor pole arc	β_r	10deg.

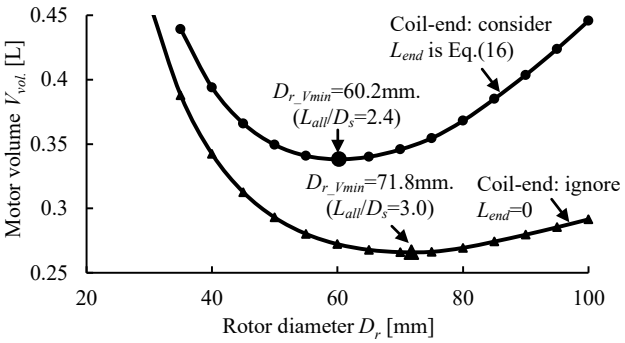

Fig. 8 Relationship between rotor diameter D_r and motor volume $V_{vol.}$

III. DESIGN EXAMPLE OF 0.75KW SRM

Table 2 shows the design requirements and constants of the design example. In the design example, P_{out} is 750W, ω_{max} is 5000r/min, and ω_{base} is 3000r/min. Therefore, T_{max} is 2.39Nm and $T_{\omega max}$ is 1.43Nm. Assuming that 35H300 is employed for the motor core; B_{sat} is 1.64T from the value of the magnetic flux density at 5000A/m in the data sheet.

A. Number of Phases and Stator- Rotor- Poles

In the design example, f_{e_max} is 2kHz. This is because the sampling frequency is assumed to be 20kHz; and the value with a margin of 1/10 is set as f_{e_max}. By calculating the Eq.(1), the condition of $N_r \le 24$ should be satisfied. Therefore, three-phase 18-12 type SRM which is the limit of the proposed method is selected according to Table 1.

B. Miniaturization design

Fig.8 shows the relationship between the rotor diameter D_r and the motor volume $V_{vol.}$. As shown in Fig.8, there is a point to minimize $V_{vol.}$ by changing D_r. This minimum point is decided by two factors as following. (i) L_h can be reduced by increasing D_r from Eq.(5) because the torque depends on the rotor size, i.e. the air gap area. (ii) D_s is inevitably increased by increasing D_r from Eq.(13) because the stator diameter is outside of the rotor diameter. Therefore, there is a trade-off relationship in two factors

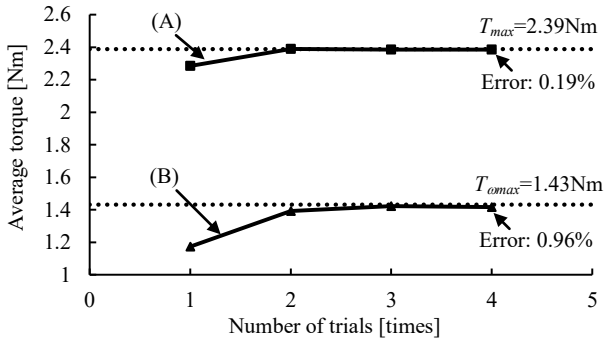

Fig. 9 Number of trials and average torque

TABLE III
DESIGN REQUIREMENTS AND CONSTRAINTS.

Main parameters		
Number of phases	m	3
Number of stator poles	N_s	18
Number of rotor poles	N_r	12
Rotor diameter	D_r	60.2mm
Stator diameter	D_s	101.4mm
Thickness of motor core	L_h	33.7mm
Overall axial length	L_{all}	41.9mm
Number of turns	N	92turns (ϕ=0.69mm)
Control parameters		
Current amplitude at operating point (A) in Fig.1	I_{Tmax}	34.1A
Current amplitude at operating point (B) in Fig.1	$I_{\omega max}$	28.4A

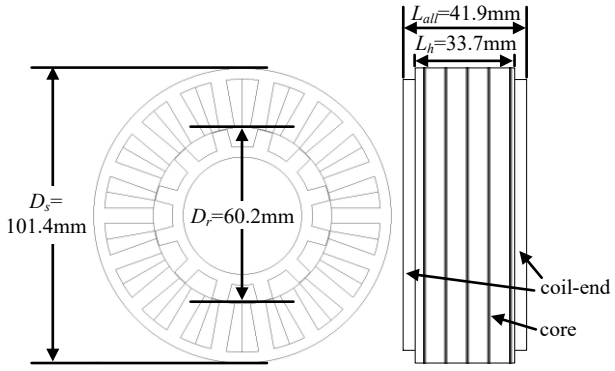

Fig. 10 Cross section of designed SRM

(i) and (ii). The point where (i) and (ii) are balanced is the minimum point of motor volume $V_{vol.}$. In addition, the ratio of L_{all}/D_s which minimizes $V_{vol.}$ is smaller in consideration of coil-end. This is because the large ratio of L_{all}/D_s, i.e. flat shape, leads to increase of the axial length of the motor due to the coil-end.

C. Parameter adjustment with FEM

Fig.9 shows the average torque when α_{Tmax} and $\alpha_{\omega max}$ are adjusted according to the algorithm explained in the subsection 2-F. The initial value of α_{Tmax} and $\alpha_{\omega max}$ is 1.5. The larger number of trials makes the average torque the desired torque and finally converges. In this case, when four trials are conducted, the error rate is 1% or less.

D. Validation of designed motor

Table 3 shows the designed motor diameters, whereas

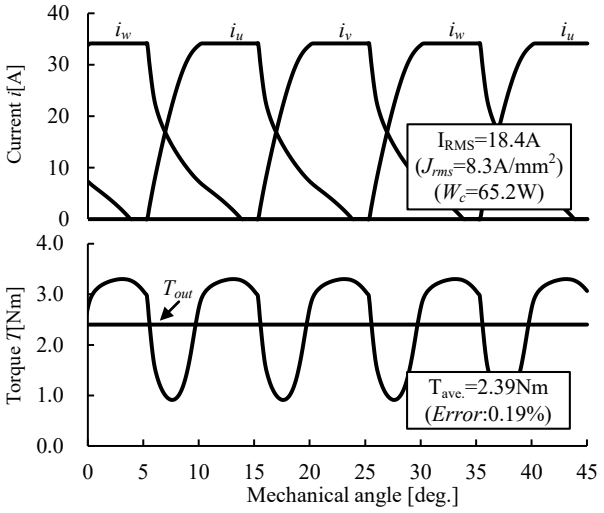

(a) Operating point (A)

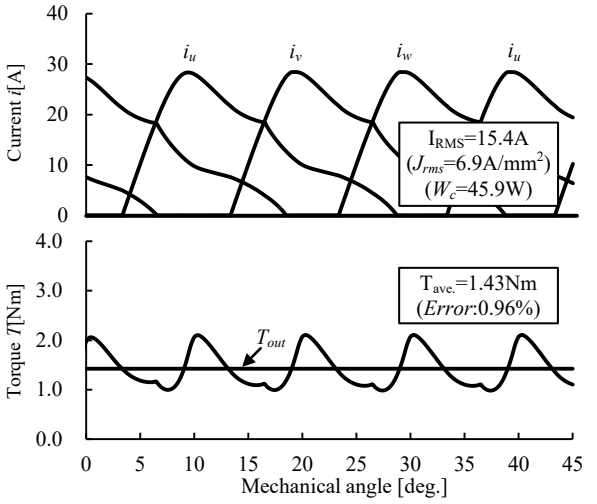

(b) Operating point (B)

Fig.11 Simulation results of currents and torques at operating points (A) and (B)

Fig.10 shows the cross section of the designed motor. The designed motor has m=3, N_s=18, N_r=12, D_s=101.4mm, D_r=60.2mm, L_h=33.7mm, N=92turns.

Fig.11 shows the simulation results at operating point (A) and (B) in Fig.1. It is confirmed that the torque with an error rate of 1% or less is obtained at each point. Note that the stator diameter is decided from the constraint of maximum copper loss. The current density is 8.3A/mm^2 for the design with 10A/mm^2, whereas the copper loss is 65.2W for the design with 75W. These difference is due to the error with Eq.(6) as explained at Fig.6.

E. Effect of magnetic saturation

Fig.12 shows the current paths at operating point (A) and point (B) in cases of α_{sat}=1.2, 1.6, 2.0. As shown in Fig.12, the selection of larger α_{sat} leads to the use of deeper magnetic saturation. Therefore, α_{sat} is the specific parameter in order to arbitrarily determine how much to use the magnetic properties of the iron material.

Fig.13 shows the relationship between the magnetic saturation level α_{sat} and the motor volume. Note that the

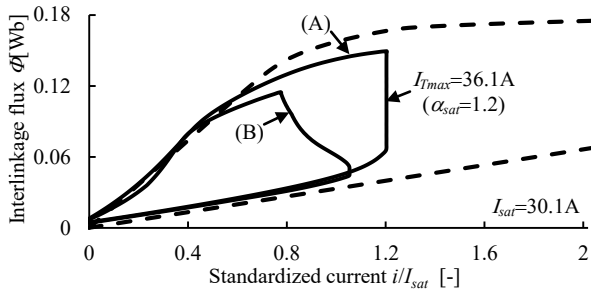

(a) magnetic saturation level α_{sat}=1.2

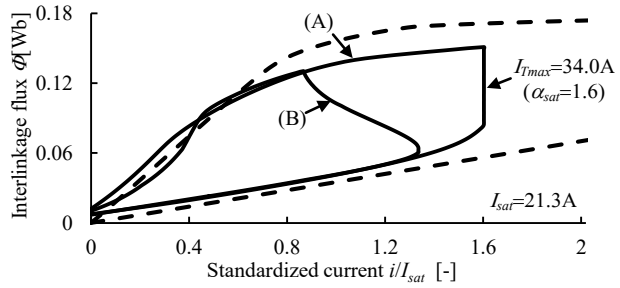

(b) magnetic saturation level α_{sat}=1.6

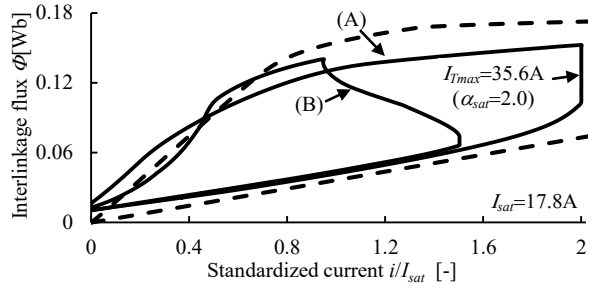

(c) magnetic saturation level α_{sat}=2.0

Fig.12 Current paths at operating point (A) and point (B) under different magnetic saturation level

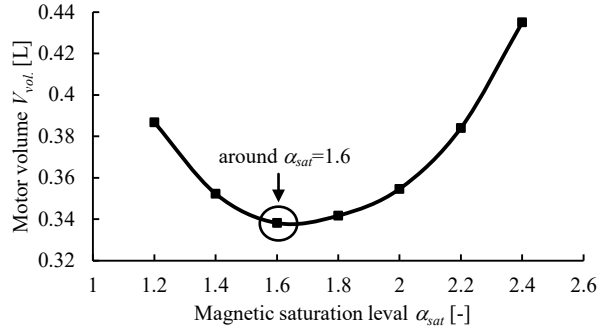

Fig.13 Relationship between magnetic saturation level α_{sat} and motor volume.

motor volume is minimized with the proposed method at each α_{sat}. As shown in Fig.13, in case of lower α_{sat} than 1.6, the motor volume is reduced thanks to active use of the magnetic properties of the iron material. On the other hand, in case of larger α_{sat} than 1.6, the motor volume is increased. This is because the selection of larger α_{sat} leads to larger ratio of L_{all}/D_s for the reduction of the current density and the copper loss. This results in increase of the axial length due to the coil-end. Therefore, in case of excessively large α_{sat}, the volume reduction effect is lower than the volume increase effect due to the coil-end. In the designed example, α_{sat}=1.6 is the best selection to satisfy the required N-T characteristic and to realize miniaturized motor volume considering the magnetic properties.

TABLE IV
DESIGN PARAMETERS.

		2605SA1 (B_{50}=1.53T)	35JNE300 (B_{50}=1.74T)
Magnetic saturation level	α_{sat}	1.8	1.6
Rotor diameter	D_r	62.6mm	59.2mm
Stator diameter	D_s	106.2mm	101.5mm
Thickness of motor core	L_h	33.8mm	30.4mm
Overall axial length	L_{all}	42.4mm	38.6mm
Number of turns	N	94turns (ϕ=0.72mm)	98turns (ϕ=0.68mm)
Motor volume	$V_{vol.}$	0.376L	0.312L

Table 4 shows the design parameters in case of employing an amorphous alloy (2605SA1) and high-grade silicon steel (35JNE300) into a motor core. The volume of the motor of 35JNE300 which has higher B_{sat} is about 17% smaller than that of 2605SA1. From the above results, it is confirmed that it is possible to optimally design the motor according to the magnetic properties of the magnetic material without output equation relying on designer's experience or past design example.

IV. CONCLUSIONS

This paper proposeed a miniaturization design method for a SRM from the requirement of N-T characteristic. In particular, α_{sat} was defined in order to arbitrarily determine how much to use the magnetic properties of the iron core material. The typical motor dimensions are obtained by setting the parameter related to magnetic saturation, maximum electrical frequency, maximum current density, maximum copper loss, conductor slot fill factor, magnetic properties of material, and input voltage. The designed motor was analyzed by a FEM in order to validate the proposed method.

REFERENCES

[1] U. U. Ekong, M. Inamori, and M. Morimoto, "Field-Weakening Control for Torque and Efficiency Optimization of a Four-Switch Three-Phase Inverter-Fed Induction Motor Drive," IEEJ Journal of Industry Applications, vol. 8, no. 3, pp. 548-555 (2019)

[2] K. Abe, H. Haga, K. Ohishi, Y. Yokokura, and H. Kada, "Source Current Harmonics and Motor Copper Loss Reduction Control of Electrolytic Capacitor-less Inverter for IPMSM Drive," IEEJ Journal of Industry Applications, vol. 8, no. 3, pp. 404-412 (2019)

[3] K. Kiyota, T. Kakishima, and A. Chiba: "Comparison of Test Result and Design Stage Prediction of Switched Reluctance Motor Competitive With 60-kW Rare-Earth PM Motor", IEEE Transactions on Industrial Electronics, vol. 61, no. 10, pp. 5712-5721 (2014)

[4] Miller T. J. E.: Switched reluctance motors and their control, pp.161-180, Magna Physics Publications and Oxford University Press (1993)

[5] Jin-Woo Ahn, Grace Firsta Lukman: "Switched reluctance motor: Research trends and overview", CES Transactions on Electrical Machines and Systems, Vol. 2, No. 4, pp. 339-347 (2019)